Molecular Crystals and Liquid Crystals

Publication details, including instructions for authors and subscription information:
http://www.tandfonline.com/loi/gmcl20

Liquid-Crystals for Tunable Photonic Crystals, Frequency Selective Surfaces and Negative Index Material Development

I. C. Khoo [a], Yana Williams [a], Andres Diaz [a], Kan Chen [a], J. A. Bossard [a], L. Li [a], D. H. Werner [a], E. Graugnard [b], J. S. King [b], S. Jain [b] & C. J. Summers [b]

[a] Electrical Engineering Department, Pennsylvania State University, University Park, Pennsylvania, USA
[b] School of Materials Science & Engineering, Georgia Institute of Technology, Atlanta, USA

Version of record first published: 22 Sep 2006

To cite this article: I. C. Khoo, Yana Williams, Andres Diaz, Kan Chen, J. A. Bossard, L. Li, D. H. Werner, E. Graugnard, J. S. King, S. Jain & C. J. Summers (2006): Liquid-Crystals for Tunable Photonic Crystals, Frequency Selective Surfaces and Negative Index Material Development, Molecular Crystals and Liquid Crystals, 453:1, 309-319

To link to this article: http://dx.doi.org/10.1080/15421400600653654

Mol. Cryst. Liq. Cryst., Vol. 453, pp. 309–319, 2006

ISSN: 1542-1406 print/1563-5287 online
DOI: 10.1080/15421400600653654

Liquid-Crystals for Tunable Photonic Crystals, Frequency Selective Surfaces and Negative Index Material Development

I. C. Khoo
Yana Williams
Andres Diaz
Kan Chen
J. A. Bossard
L. Li
D. H. Werner
Electrical Engineering Department, Pennsylvania State University, University Park, Pennsylvania, USA

E. Graugnard
J. S. King
S. Jain
C. J. Summers
School of Materials Science & Engineering, Georgia Institute of Technology, Atlanta, USA

We present the results of experimental and theoretical studies that demonstrate the feasibility of realizing electro-optical switching, frequency filtering and negative index of refraction. In liquid crystal infiltrated TiO_2 inverse opal 3-D photonic crystals, we observed a sizeable electrical tuning of the Bragg reflection peak. In frequency selective structures with a liquid crystal over-layer, the tuning range can be as wide as 380 nm, operational throughout the entire visible – far infrared spectra range. Furthermore, some of the structures can be designed to exhibit a negative index of refraction property over a predetermined frequency interval.

Keywords: frequency selective surfaces; liquid crystals; negative index materials; photonic crystals; tunable reflection and transmission

This work is supported by the Air Force Office of Scientific Research, the Army Research Office, and the NSF-MRSEC Center for Nanoscale Science under grant number DMR-0213623. We acknowledge helpful discussions with T. Mallouk and V. Shalaev.

Address correspondence to I. C. Khoo, Electrical Engineering Department, Pennsylvania State University, University Park, PA 16802, USA. E-mail: ick1@psu.edu

I. INTRODUCTION

Current research and development in electro- and nonlinear-optical materials for photonic applications are largely centered on nanostructured materials that exhibit unique physical and optical properties [1–4]. For practical usage, it is highly desirable to introduce tunability in the structure/device. In this respect, liquid crystals clearly stand out as the preferred means of achieving tunability as they possess extraordinarily large electro-optics and nonlinear optical responses. They are also compatible with almost all widely used optoelectronic materials and possess very broadband [UV-far infrared] transparency and large optical birefringence Δn [6]. Their fluid nature allows easy incorporation into various geometries and nm-scale pore sizes [7]. In this paper, we report successful demonstrations of tunable reflective and transmissive optical elements based on liquid crystal impregnated photonic crystals [LC-PC], and liquid crystals on planar frequency selective structures [LC-PFSS]. Furthermore, we also show that the latter is capable of exhibiting negative index of refraction at any desired frequency of operation over the entire visible – far infrared spectrum.

II. LC INFILTRATED PHOTONIC CRYSTALS

Photonic crystals in 1-, 2- and 3-D forms have received intense research interests owing to the rich variety of possibilities in terms of material compositions, lattice structures and their electronic as well as optical properties [1,2,7]. By using active tunable material as a constituent, photonic crystals can function as tunable filters, switches and lasing devices. In particular, liquid crystals have been employed in many studies involving opals and inverse opal structures. However, most of the tuning mechanisms are via thermal means, which are slow and not suitable for practical devices. Also, the tuning range is quite limited, as a result of the relatively small volume fraction of the tunable material.

We have recently [8] studied large-pore inverse opal photonic crystal structures impregnated with nematic liquid crystal. Because of the higher volume fraction for NLC infiltration, a much larger tuning range [>20 nm] of the Bragg reflection peak can be achieved. Figure 1a–b show the calculated band structures of a liquid crystal infiltrated inverse opal photonic crystal. The structure considered is an inverse 6-μm thick fcc structure of anatase (TiO_2) with a 43% open volume fraction. The pore diameter r is 208 nm, with lattice constant a satisfying $r/a = 0.35$. The TiO_2 framework refractive index is

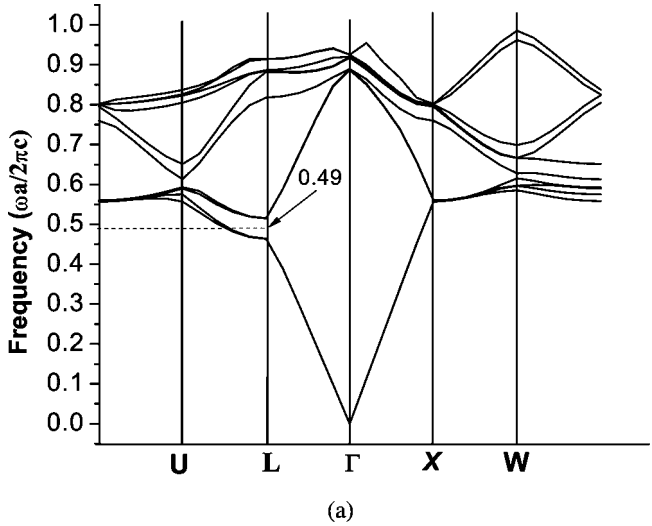

(a)

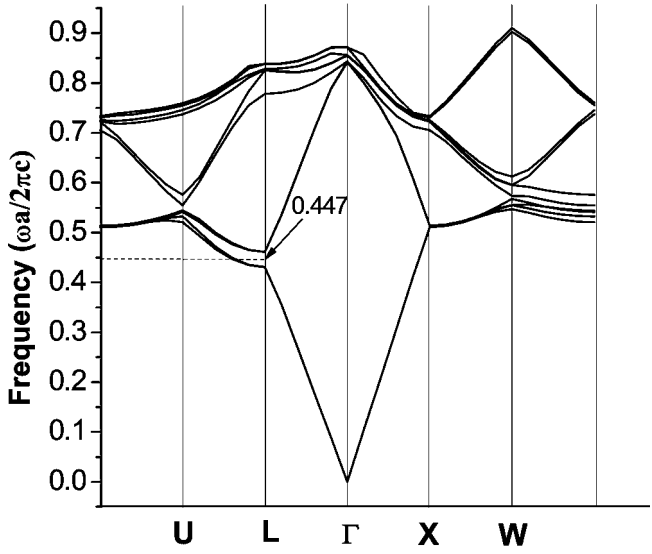

(b)

FIGURE 1 (a) Band structure of TiO_2 replica when the refractive index of NLC $n_{LC} = 1.5$ (b) Band structure of TiO_2 replica when the refractive index of NLC is $n_{LC} = 1.7$.

$n_T = 2.43$, while the NLC refractive indices are $n_o = 1.5$ and $n_e = 1.7$ for field polarized perpendicular and parallel to the NLC director axis, respectively. Changing the LC director axis orientation changes the dielectric contrast ratio from $n_T/n_o = 2.43/1.5 = 1.62$ to $n_T/n_e = 2.43/1.7 = 1.43$. This dielectric contrast change is reflected in changes in the band structures, as illustrated in Figure 1a–b. For example, the band gap between the 2nd and 3rd band at the L wavevector in Figure 1a is larger than the band gap in Figure 1b ($\Delta\omega_a = 0.056 > \Delta\omega = 0.031$), and the position of the mid-gap is also shifted ($\omega_a = 0.49 > \omega_b = 0.447$), i.e., the bandgap can be tuned [widened and shifted] as the LC director axis orientation within the voids is realigned by an applied ac field.

The large-pore inverse opals are synthesized by a standardized technique [9]. A 10-μm thick opal template was fabricated by direct self-assembly of mono-dispersed polystyrene spheres (329 nm diameter, Duke Scientific) using a confinement cell technique. The template was sintered for 1 hour at 100°C to increase the diameter of the sphere contact points and reduce the air void volume. The sintered template was infiltrated with amorphous TiO_2 (refractive index = 2.30) using atomic layer deposition (ALD) as reported elsewhere [10], but with the temperature lowered to 80°C and the cycle times extended to allow for complete diffusion within the sintered template. For ALD within an un-sintered template, the maximum filling fraction is achieved at 86% of the pore volume (or 22.4% of the total volume), due to the closure of the pores in the (111) direction. The fully infiltrated opal was next ion-milled to remove the top half of the outer most layers of spheres, which provided access to the interconnected polystyrene lattice. The sample was immersed in toluene overnight to completely remove the polystyrene template, forming a low filling fraction open inverse opal, c.f. Figure 2.

Compared to both opals and conventional inverse opals, this open structure provides a much less constricting volume for LC reorientation under applied fields, which should facilitate the largest possible optical tuning. The sample was infiltrated with liquid crystal (5CB) using capillary forces with both the sample and the LC at ~50°C [>Tc of 32°C]. The reflectance spectra of the sample were measured as a function of applied square wave electric modulation at 25 kHz. At zero bias, the Bragg peak of the sample was observed at 882 nm, c.f. Figure 3. With applied bias, the Bragg peak was continuously shifted toward the UV. A maximum shift of 15 nm to 867 nm was observed for an ac applied field amplitude of 50 V. To 'loosen' the pinning effect of the liquid crystals, we have coated the inner surfaces of some of the inverse opals with hydrophobic agent. A similar Bragg

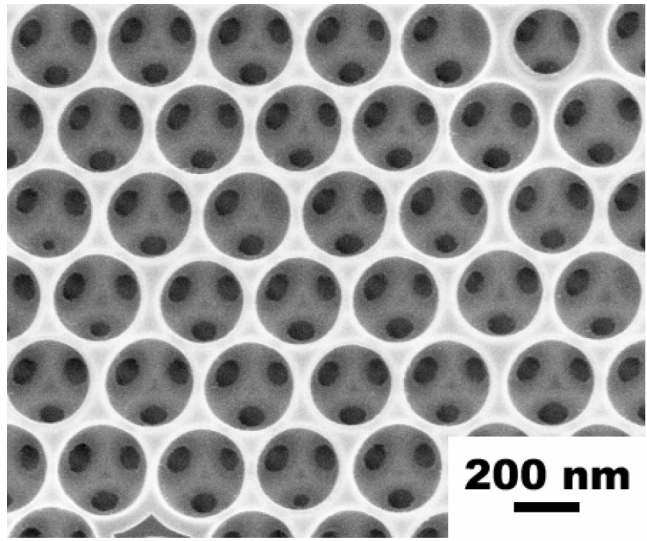

FIGURE 2 SEM photograph of the TiO_2 inverse opal photonic crystal fabricated.

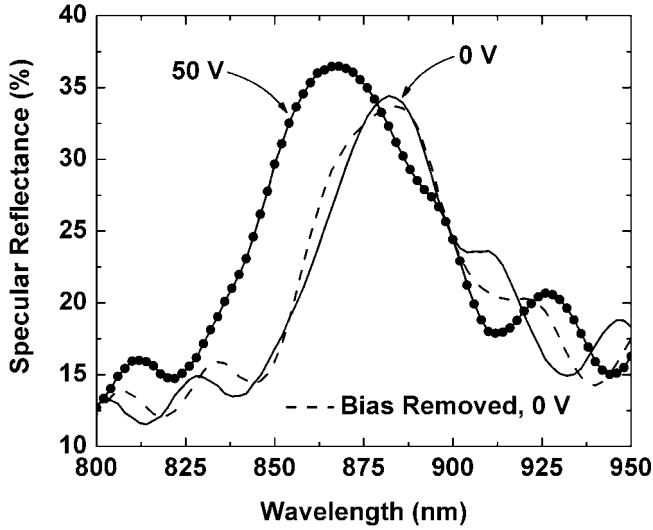

FIGURE 3 Experimentally observed electrical tuning of the Bragg reflection peak from the NLC infiltrated TiO_2 inverse opal photonic crystal.

reflection tuning experiment showed that the tuning range is increased to ~ 20 nm at a maximum applied voltage of 50 V.

In ongoing experiments, we are investigating the infiltration of these inverse opal structures with large-birefringence NLC to increase the tuning range. We are also studying nano-particulates doped liquid crystals with extremely high optical nonlinearity [characterized by optical intensity dependent refractive index change coefficient $\sim 10^{-2}\,\mathrm{cm}^2/\mathrm{W}$] to explore the possibility of tuning by optical means [11,12].

III. TUNABLE FREQUENCY SELECTIVE PLANAR STRUCTURES [FSPS]

We have recently also investigated optical filters and tunable reflective/transmissive devices based planar frequency selective structures [PFSS], often also referred to as frequency selective surfaces [4]. PFSS are two-dimensional periodic arrays of metallic patches or aperture elements that possess low-pass, high-pass, band-pass, or multi-band filtering properties for incident electromagnetic waves [13]. Total reflection or total transmission will occur when the wavelength corresponds to the "resonant length" of the PFSS screen elements. The pattern of metallic patches on the dielectric substrate is designed by a genetic algorithm (GA) technique. Details of the GA may be found in previous studies [3,13]. Briefly, we represent the parameters of a frequency selective surface (e.g., unit cell size, unit cell geometry, substrate and superstrate properties, etc.) in a binary string called a chromosome. The initial population is created by randomly generating N binary strings of the correct length, where N is the population size. Each population member is evaluated for fitness by translating the genetic data encoded in the chromosome into PFSS design parameters and simulating the response of the PFSS using a full-wave Periodic Moment Method (PMM) code [4,13].

To realize low loss visible/IR PFSS, one approach is to replace the metallic portion of the FSS screen with suitable dielectric materials which have much less loss in the visible/IR. We have also developed [13] a full-wave Periodic Finite Element Boundary Integral (PFEBI) code which is capable of accurately modeling homogeneous as well as inhomogeneous dielectric PFSS structures. The PFEBI approach is computationally efficient and therefore can be used in conjunction with a robust optimization technique such as the genetic algorithm (GA). An exemplary structure design is given in Figure 4a that will function as an excellent polarization independent optical filter at 600 THz (0.5 μm). The unit cell size of the PFSS is $0.393\,\mu\mathrm{m} \times 0.393\,\mu\mathrm{m}$,

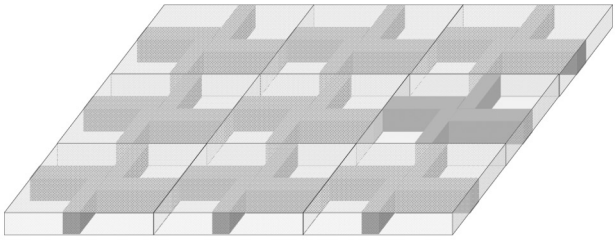

(a)

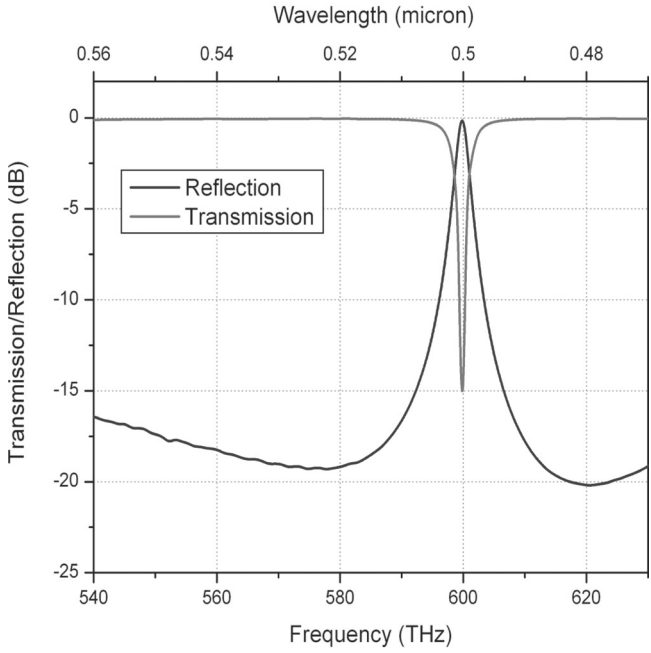

(b)

FIGURE 4 (a) Example of an all-dielectric polarization independent FSS 600 THz [$\lambda = 0.5\,\mu m$] stop-band filter. (b) Transmission [upper curve] and reflection [lower curve] spectra for the all-dielectric FSS.

with a thickness of 0.172 μm and consists of two different dielectric materials in the same layer with $\varepsilon_{r1} = 1.82$ and $\varepsilon_{r2} = 2.82$. The response for this polarization independent all-dielectric PFSS is shown in Figure 4b, which shows a sharp transmission dip or stop-band centered at the desired (designed) wavelength of 0.5 μm.

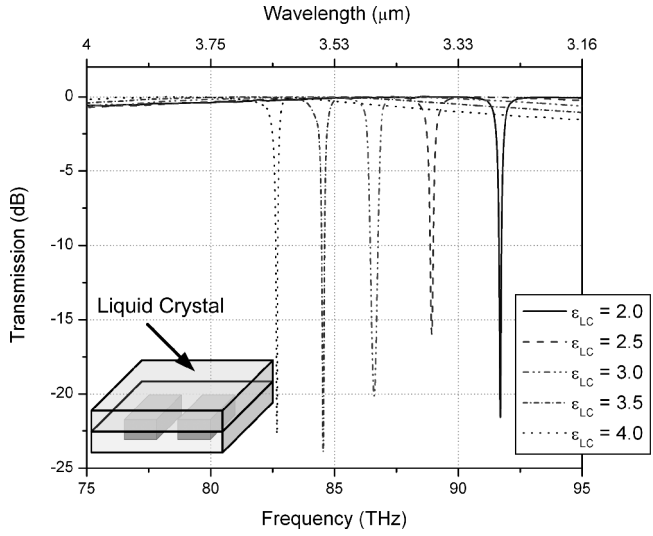

FIGURE 5 Transmission spectra of an all-dielectric PFSS with a liquid crystal over-layer as the optical dielectric constant of the NLC is changed from 2 to 4 [right to left].

The planar geometry of the PFSS allows easy incorporation of a liquid crystal overlayer. The dimensions of the PFSS unit cell as shown in the insert of Figure 5 are $3.04\,\mu m \times 3.04\,\mu m$. The PFSS is composed of polyimide ($\varepsilon_{r1} = 2.6$) blocks [$1.14\,\mu m \times 1.52\,\mu m$] embedded in a layer of silica ($\varepsilon_{r2} = 3.9$) with a $1\,\mu m$ overlayer of liquid crystal. Both the polyimide blocks and silica have a thickness of $1.0\,\mu m$. As shown in Figure 5, by changing the dielectric constants of the LC from 2 [$n_0 = 1.414$] to 4 [$n_e = 2$], the stop-band in the transmission response can be shifted from 92 THz [$\sim 3.26\,\mu m$] to 83 THz [$3.64\,\mu m$], i.e., a tuning range of 380 nm for a birefringence Δn of 0.6. Accordingly, since the birefringence of nematic liquid crystals span the entire visible to far infrared spectrum, LC-PFSS will allow us to design and fabricate very broadband high-extinction-ratio tunable filters/switches.

IV. NEGATIVE INDEX OF REFRACTION

In effect, PFSS replicates the frequency selectivity of 3-D photonic crystal, by means of diffraction from a 2-D pattern. The pattern design is guided by the desired optical properties such as the transmission band location, and the resulting complex refractive index n of the

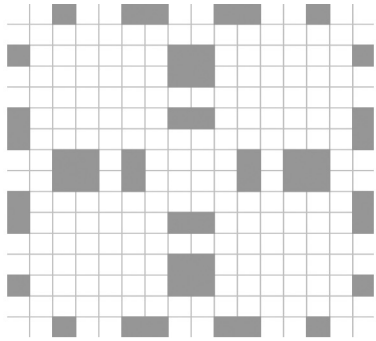

(a)

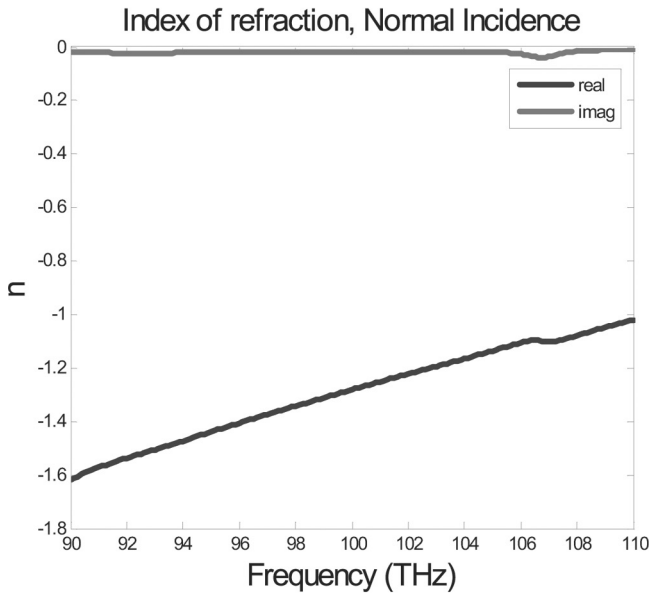

(b)

FIGURE 6 (a) PFSS unit cell structure for operation at the optical regime [wavelength around 3 μm]. (b) Plot of the real [lower curve] and imaginary [upper curve] parts of the refractive index of the PFSS structure showing negative index property and low loss.

PFSS. In structural form, PFSS is the short-wavelength-metallo-dielectric-equivalent of metallic dipole/split-ring structures that exhibit negative index of refraction [14–16] in the microwave, both

structures being based on exploiting the (metallic) plasmonic resonances and dispersion of the metallic component with a dielectric background. The PFSS, however, have the important advantage that their planar designs can be easily scaled from the microwave and millimeter wave through the IR and to visible wavelengths using conventional micro- and nano-fabrication techniques.

Using a GA approach, we succeeded in designing a metallo-dielectric PFSS that exhibits a negative index of refraction in the near IR regime. The structure design is given in Figure 6a and consists of a 150 nm thick metallic (Ag) 'screen' sandwiched symmetrically by two 0.508 μm thick polymeric [polyimide] films. The unit cell size of the FSS is 2.75 μm × 2.75 μm. At the frequency around 100 THz, the dielectric constant of Ag is $\varepsilon_{Ag} = -390.8 - 48.84i$, whereas the dielectric constant of polyimide is $\varepsilon_p = 2.63$ [with very small imaginary part, i.e., low loss]. As shown in Figure 6b, for this PFSS design the real part of the refractive index is negative [ranging from -1.6 to -1.0], while the imaginary part of the refractive index is ~ 0 for the frequency interval investigated i.e., we have a very low loss negative index material [NIM]. By incorporating liquid crystal as an overlayer onto these NIM structures, it is clearly feasible to design LC-NIM at any desired frequency in the entire visible-infrared regime. Since the dielectric constant of the liquid crystal can be electrically modulated, these NIMs possess the interesting and potentially very useful property that they can be switched between the positive and the negative index states.

V. CONCLUSION

In conclusion, we have demonstrated by theory and experiments the feasibility of realizing widely tunable LC- photonic crystal and planar frequency selective structures, and negative index materials/optical elements. These liquid crystal optical elements/devices enjoy low loss, multi-functionality and are electrically or optically reconfigurable and tunable over a very broad spectrum ranging from the visible through the infrared to the microwave regime.

REFERENCES

[1] Mach, P., Wiltzius, P., Megens, M., Weitz, D. A., Lin, K.-H., Lubensky, T. C., & Yodh, A. G. (2002). *Phys. Rev. E*, *65*, 031720.

[2] Mertens, G., Röder, T., Schweins, R., Huber, K., & Kitzerow, H.-S. (2002). *Appl. Phys. Lett.*, *80*, 1885–1887.

[3] Bossard, J. A., Werner, D. H., Mayer, T. S., & Drupp, R. P. (2005). *IEEE Transactions on Antennas and Propagation*, *53*(4), 1390–1400, and references therein by D. H. Werner et al.

[4] Drupp, R., Bossard, J., Werner, D. H., & Mayer, T. S. (2005). *Appl. Phys. Letts.*, *86*, 081102. (3 pages).
[5] Wu, T. K. (Ed.). (1995). *Frequency Selective Surface and Grid Array*, Wiley & Sons: New York.
[6] Khoo, I. C. (1995). *Liquid Crystals: Physical Properties and Nonlinear Optical Phenomena*, Wiley InterScience: NY.
[7] Larsen, T. T., Bjarklev, A., Hermann, D. S., & Broeng, J. (2003). *Optics Express*, *11*, 2589–2596.
[8] Graugnard, E., King, J. S., Jain, S., Summers, C. J., Zhang-Williams, Y., & Khoo, I. C. (2005). *Phys. Rev. B*, *72*, 233105.
[9] Park, S. H., Qin, D., & Xia, Y. (1998). *Adv. Mater*, *10*, 1028–1032.
[10] King, J. S., Graugnard, E., & Summers, C. J. (2005). *Adv. Mater.*, *17*, 1010–1013.
[11] Khoo, I. C., Ding, J., Zhang, Y., Chen, K., & Diaz, A. (2003). *Appl. Phys. Letts.*, *82*, 3587–3589.
[12] Khoo, I. C., Williams, Y. Z., Lewis, B., & Mallouk, T. (2005). *Mol. Cryst. Liq. Cryst.*, *446*, 233–244.
[13] Bossard, J. A., Werner, D. H., Mayer, T. S., Smith, J. A., Tang, Y. U., Drupp, R. P., & Ling Li. (2006). IEEE Transactions on Antenna and Propagation, Vol. 54, pp. 1265–1276.
[14] Podolskiy, V. A., Sarychev, A. K., & Shalaev, V. M. (2002). *J. Nonlinear Opt. Physics and Materials*, *11*, 65–74.
[15] Podolskiy, V. A., Sarychev, A. K., & Shalaev, V. M. (2003). *Optics Express*, *11*, 735–745.
[16] Schonbrun, E., Tinker, M., Park, W., & Lee, J.-B. (2005). Negative index of refraction has also been observed in photonic crystal. *IEEE Photon. Technol. Lett.*, *17*, 1196.